Microsystem Technologies
https://doi.org/10.1007/s00542-020-04947-x

TECHNICAL PAPER

A fast-sensing readout circuit in 240 Hz enabled by code division multiple access (CDMA) implemented for an ultra-thin on-cell flexible capacitive touch panel

Chia Yu Chang[1] · Paul C.-P. Chao[1,2] · Jeremy H.-S. Wang[1] · Ying Cheng Su[1] · Smriti Thakur[1] · Tse-Yi Tu[1,3]

Received: 15 December 2019 / Accepted: 25 June 2020

Abstract
A new fast readout circuit employing the known coding scheme of code division multiple access (CDMA) is successfully designed and applied to a 7-inch ultra-thin, flexible on-cell touch screen panel (TSP). The adopted CDMA is known originally as a coding scheme for data communication, which is applied in this study to address the sensing electrodes of the ultra-thin flexible touch panel. Due to the orthogonality between the driving signals to the touch panel coded by Walsh transform, one type of CDMA, the interference noises between sensing electrodes can be reduced effectively to render accurate touch sensing results. The electromagnetic interference from the flexible display can also be filtered out as baseline component in the output signal. And the frame time of touch reporting can be substantially shortened. Following the sensing electrode is a new readout designed of the switched-capacitor (SC) circuit, to avoid distributing sample signals from parasitic capacitance and also to enlarge the voltage changes due to the capacitance changes caused by touches. A 12-bit analog-to-digital converter (ADC) is orchestrated after the SC circuit to transform the front-end analog signal to digital codes. The digital part of the designed readout adopts a correction algorithm to eliminate the background signals from the display, and also a moving average algorithm to minimize the higher-frequency noises from the display and other electrodes. Experiments are conducted to validate the expected performance. It is evidenced that the Walsh code driving algorithm improves the quality of the readout output signal to be in 42 dB SNR, the report rate to a fast 240 Hz, and a power consumption of 0.39 mW by each sensing channel.

1 Introduction

For many commercial mobile devices nowadays, such as smart bracelets, smartwatches and mobile phones, a touch screen panel (TSP) on the displays has become a must component for the aforementioned devices to interact with users. The operation principles adopted by the TSP can be optical, acoustic, capacitive, or resistive (Dieulesaint et al. 1991; Downs 2005). Among all the principles, the projective capacitive touch sensing provides high sensitivity of touch detection, thus preferred in many applications (Cordeiro et al. 2013; Barrett and Omote 2010; Ko et al. 2010). Recently, there is an increasing demand for capacitive touch screens to own the features like flexibility and lightweight. To this end, on-cell TSPes have been promising candidates to achieve flexibility of the TSP, since the distance between the Indium Tin Oxide (ITO) electrode and the display panel of an on-cell touch panel can be reduced to about 25 μm. This 25 μm is way below the traditional out-cell TSP's 700 μm (Jang et al. 2013). On the other hand, for the total flexibility of mobile devices display, the display adopted is usually the active-matrix organic light-emitting diodes (AMOLED) display (Martin et al. 2002). However, with a very thin and flexible TSP on a flexible AMOLED display, the driving and sensing signals of the TSP are subjected to strong electromagnetic interference (EMI) from the AMOLED display under in

✉ Paul C.-P. Chao
pchao@mail.nctu.edu.tw

[1] Department of Electrical Engineering, National Chiao Tung University, Hsinchu 300, Taiwan

[2] Center for Intelligent Drug Systems and Smart Bio-devices (IDS2B), National Chiao Tung University, Hsinchu 300, Taiwan

[3] Department of Mechanical Engineering, Chun Yuan Christian University, Chung Li 320, Taiwan

Published online: 02 July 2020

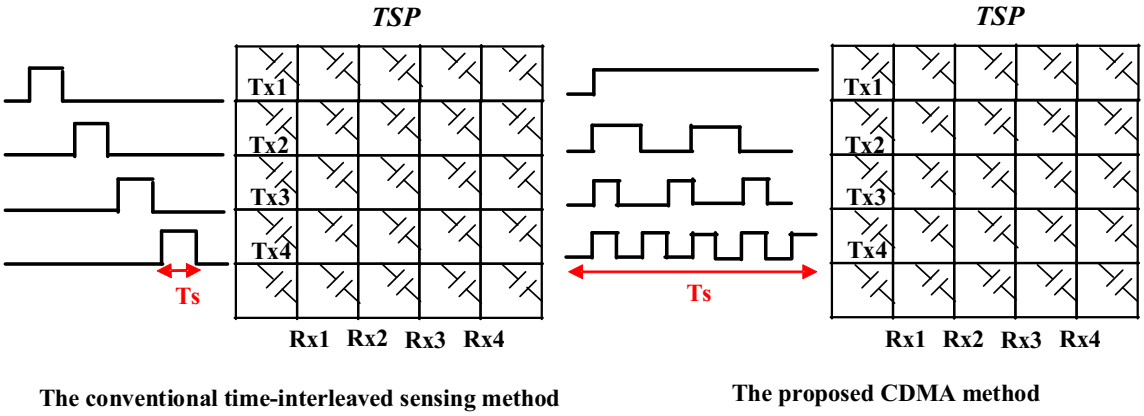

Fig. 1 The conventional and proposed sensing methodologies

operation. In addition to the EMI noises from the thin, flexible AMOLED display, there is serious parasitic capacitance effect due to the couplings between electrodes in the thin TSP and between the thin TSP and the thin AMOLED display (Jang et al. 2013), leading to the problem of constant saturation in the rear-end readout circuit. Most recently, (Park et al. 2019) presented a touch readout with 64% reduced-power via adiabatic driving over heavily coupled touch screen, but only at 120 Hz report rate. Xing et al. (2019) presented a readout circuit for the TSP capacitance in large size, the achieved specifications of which are different from the ones the current study aims for Ko (2020) proposed the readout design with in-band noise immunity with power consumed up to as high as 11.5 mW.

In this study, efforts are dedicated to design the layers of the TSP, the geometry of the conducting ITO electrode on the TSP, and the readout circuitry to optimize the signal-to-noise ratio of the output signal of the readout and avoid saturation of readout signals to achieve effective touch sensing with ultra-thin, flexible TSP. A new sensing readout circuit is designed by this study with adoption of the switched-capacitor (SC) architecture to prevent the afore-mentioned saturation caused by the large parasitic capacitance. Also, this study proposes a new driving method of code division multiple access (CDMA) (Baier 1996; Shin et al. 2013) in Walsh transform code. Note that this driving technique is realized with a novel Walsh transform code, different from Shin et al. (2013), and a new switched-capacitor circuit design to eliminate touch panel noise and to avoid saturation. The driving waveforms of CDMA are different from the conventional time-interleaved method, as illustrated by Fig. 1, where the access time (T_s) to measure mutual capacitance (C_m) between electrodes is longer by CDMA to reduce the noise. It is obvious that as the number of sensing nodes increases with larger display sizes, the method of time-interleaved method decreases significantly the frame rate, degrading the performance of the TSP (Shin et al. 2013). On the contrary, the CDMA in Walsh code (Chawla and Singh 2014) proposed by this study drive all the sensing electrodes in the TSP simultaneously with orthogonal waveforms, as shown in Fig. 1. In this way, the interference noises between electrodes can be reduced significantly due to the orthogonality, while those from the display can also be filtered out as baseline component in the output signal, not to mention that the frame time of touch reporting can be

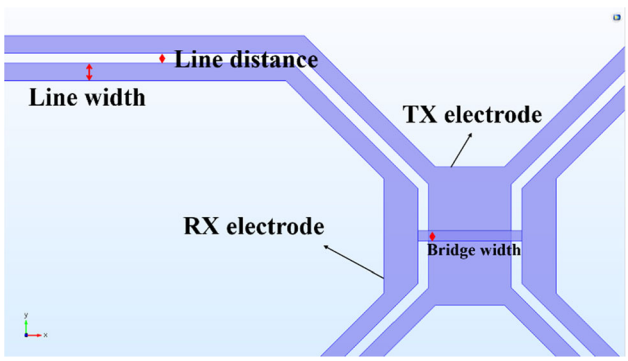

Fig. 2 The top view of the designed touch electrode geometry

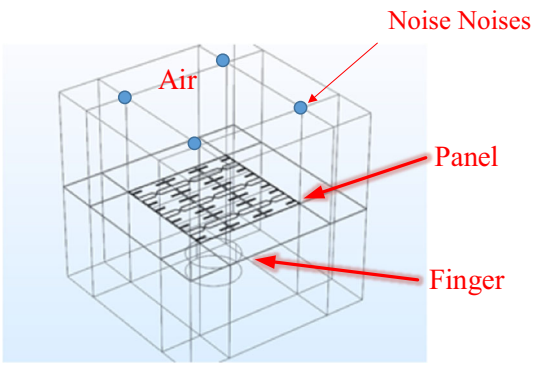

Fig. 3 The model of the touch sensing panel (TSP) in an air chamber for electro-magnetic simulation via COMSOL

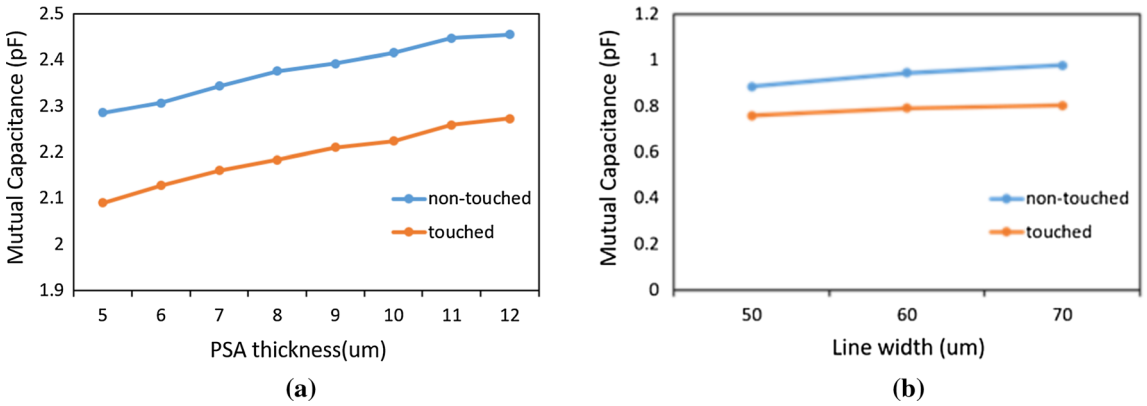

Fig. 4 **a** Mutual capacitance versus the PSA thickness. **b** Mutual capacitance versus the line width

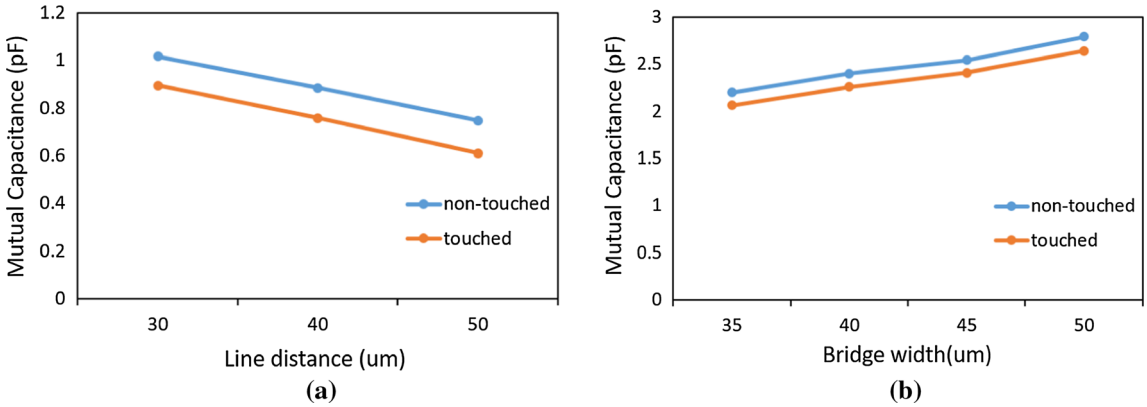

Fig. 5 **a** Mutual capacitance versus the line distance. **b** Mutual capacitance versus the bridge width

Table 1 The effects of parameters on the touch panel

	Thickness of PSA	Bridge width	Line width	Line distance
Baseline	↑	↑	↑	↓
△C	–	–	↑	↑

↑ direct proportion, ↓ inverse proportion, – unrelated

substantially shortened. The final performance of the TSP and the readout circuitry designed by this study results in 42 dB SNR for the output signal of readout, the reporting rate of 240 Hz, and an power consumption of 0.39 mW by each channel.

This paper is organized as follows. Section 2 lays out the electrode structure of the new flexible touch screen panel (TSP), followed by the determination of the important parameters of the TSP for maximizing its sensing performance. Section 3 presents the design of the readout circuitry, including the analog front-end part with multiple charge amplifiers driven by the approach of code-division multiple-sensing (CDMS) and then a digital unit with algorithms to detect touches. Section 4 shows experimental validation. Section 5 concludes this work.

2 Modeling and design of the touch screen panel (TSP)

A novel pattern of sensing electrodes as shown in Fig. 2 has been successfully designed for the ultra-thin on-cell flexible capacitive touch screen panel (TSP). The software of COMSOL's Finite Element Methods (FEM) solver is utilized to analyze characteristic for several conditions. The mutual capacitances between driving and sensing electrodes (TX and RX, respectively) are simulated to determine if there is touch. The approximate expression for the mutual capacitance between two electrodes can be captured by

Table 2 Design results

	Thickness of PSA (μm)	Bridge width (μm)	Line width (μm)	Line distance (μm)	Capacitance of non-touched (pF)	Capacitance of touched (pF)
The originals	12	30	60	40	2.40	2.28
Designed	5	40	50	30	2.40	2.26

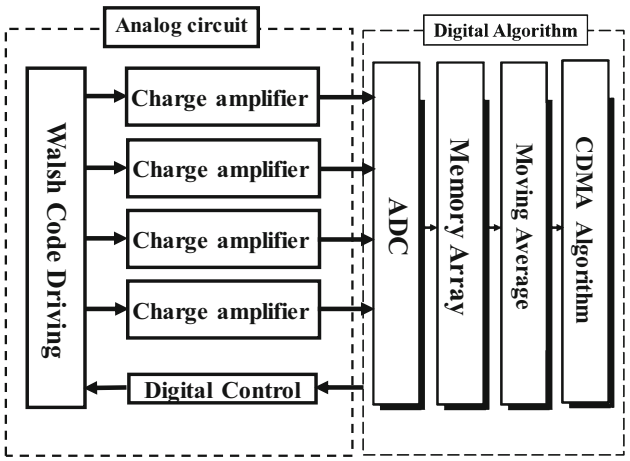

Fig. 6 Readout circuitry in blocks

$$C_m = \in_0 \in_r \frac{A}{d}, \tag{1}$$

where $\in_r$ is the relative permittivity of the capacitor dielectric material, A is the area over the overlapped electrodes, and d is the distance between two electrodes. However, this formula is established based on the assumption that two electrodes should be two parallel and without fringing field effect considered. To remedy the aforementioned problem, the mutual capacitances are captured based on the energy method, which is given by

$$C_{ii} = \frac{2}{V_i^2}\int W_e d\Omega;\ V_j = \begin{cases} 0 & j \neq i \\ V_i & j = i \end{cases}, \tag{2}$$

$$C_{ii} = \frac{2}{V_i V_j}\int W_e d\Omega - \frac{1}{2}\left(\frac{V_i}{V_j}C_{ii} + \frac{V_j}{V_i}C_{jj}\right);\ V_k = \begin{cases} 0 & k \neq i,j \\ V_i & k = i \\ V_j & k = j \end{cases}, \tag{3}$$

where V_i is electric potential, W_e is energy density, and Ω is solid angles. With the above equations, the mutual capacitances between the driving and sensing electrodes can calculated based on an FEM model established fort eh TSP, as shown in Fig. 3. To conduct the simulation initial and boundary conditions are set beforehand, such as initial values, floating and grounding and the parameters of materials, such as resistance and relative permittivity of each layer. Note also that although there is no ultra-thin displays considered in the COMSOL FEM model, but the interfering electromagnetic effects from the display are measured beforehand and modeled as noise current sources in the COMSOL model, as shown in Fig. 3, to ensure the ratio of $\Delta C/C_o$ (C_o is the baseline C; ΔC is the capacitance changes with a touch) large enough to work against noises from the display. Finally, by meshing the geometry of the TSP, a finite element model can be successfully established. With this model, all mutual capacitances can be obtained to maximize the ratio of $\Delta C/C_o$ via changing the geometry of electrodes and the thickness of each layer with given different materials in the ultra-thin TSP.

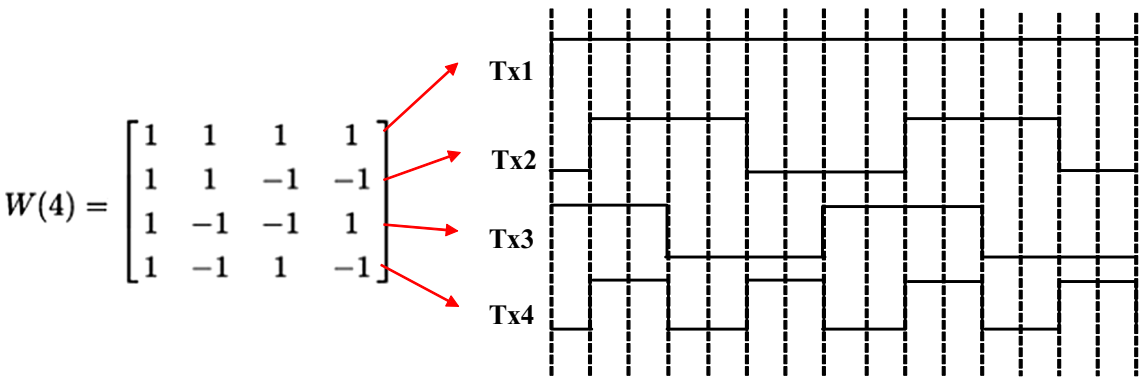

Fig. 7 The Walsh transform matrices and its timing diagram

Table 3 Comparison between the proposed CDMA and the conventional Time-interleaved sensing methods

	CDMA	Time-interleaved sensing
Driving Method	Simultaneous	Interleaved
Signal	Strong	Weak
Access time (T_s)	Long	Short
Orthogonality	Yes	No
Noise Inhibition	Eliminate the channel noise and reduce the EMI noise	Increase the integration time and reduce noise
Design	Complicated	Easy

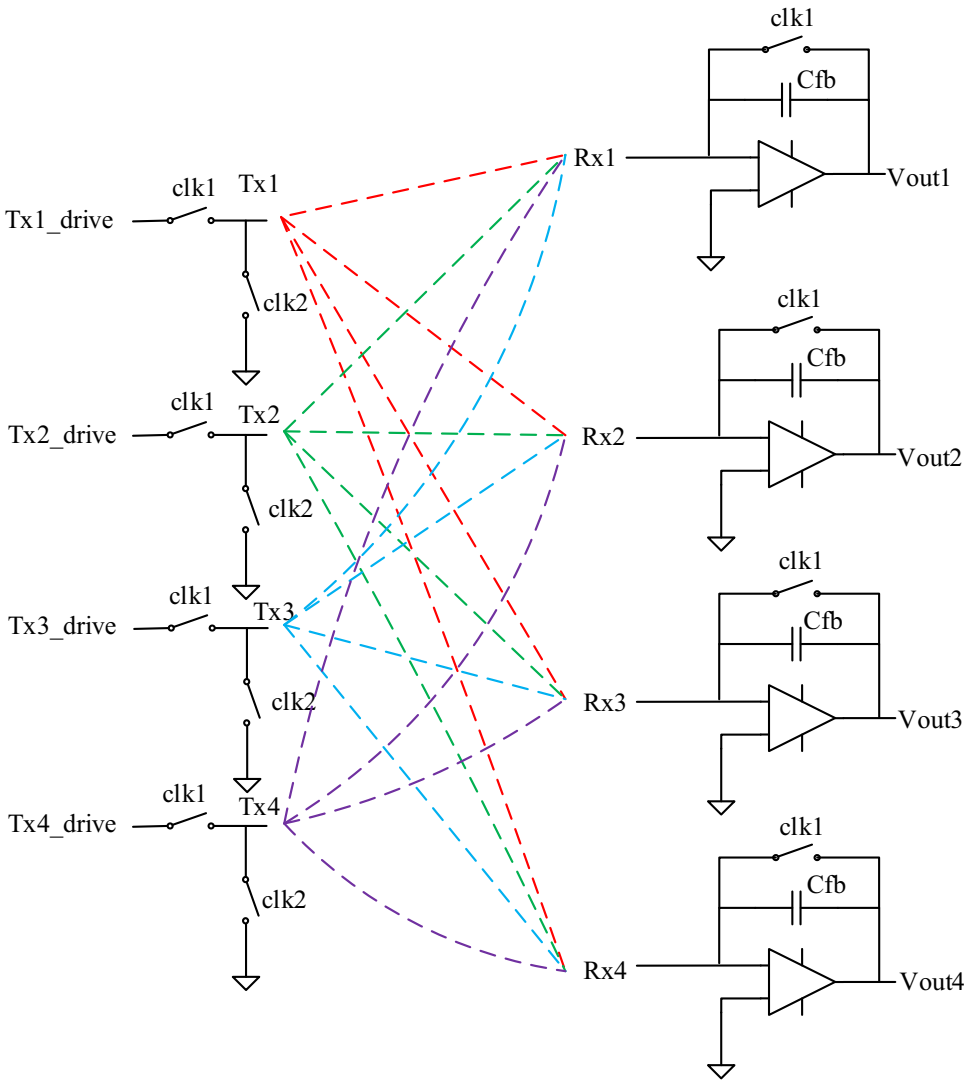

Fig. 8 The circuit topology and operations of the designed charge amplifier (CA)

To achieve the design goal of the ultra-thin TSP, the focus is on optimizing the layer thickness of pressure-sensitive adhesive (PSA) for maximum ratio of $\Delta C/C_o$. This PSA layer is to bond the touch electrode layer to display, the thickness of which affects substantially the level of electromagnetic inferencing (EMI) from the display to the touch electrode layer. The design approach herein is to find the minimum thickness of PSA possible such that only allowable EMI from display to the touch electrodes while the TSP keeps its ultra-thin property to be flexible. Simulations based on the FEM model via COMSOL are conducted to find the aforementioned minimum

thickness of PSA. Figures 4 and 5 show related simulation results. It is seen from Fig. 4a that a decrease in the PSA thickness leads to also a decrease in the mutual capacitance between the TX and RX electrodes, while the mutual capacitance is relatively constant as opposed to electrode line width, as seen in Fig. 4b. In the next step, the dependences of the mutual capacitance on the distance between electrode lines and the bridge width as defined in Fig. 2 are also explored by simulations. The results are shown in Fig. 5a, b. It can be seen from these figures that the mutual capacitance decreases as the electrode line distance increase, increasing as the bridge width increases. Table 1 summarize the dependences of baseline C_o and ΔC on the PSA thickness, bridge width, electrode line width and distance based on simulations. It is pertinent to note herein that all the parasitic (coupling) capacitances and resistances attributing to the mutual capacitances between TX and the RX electrodes are well captured into the aforementioned baseline C_o and ΔC.

With all the simulation results as shown in Table 1, it can be concluded that to achieve our goal of a thin, flexible TSP while keeping the expected performance, the thickness of PSA is reduced, while keeping the baseline C_o at adequate level by increasing the bridge width. Also, the electrode line width and distance are increased at the same time to increase ΔC. In this way, an ultra-thin, flexible touch with the expected performance offered, a maximized ratio of $\Delta C/C_o$, can be achieved. The final designs are listed in Table 2.

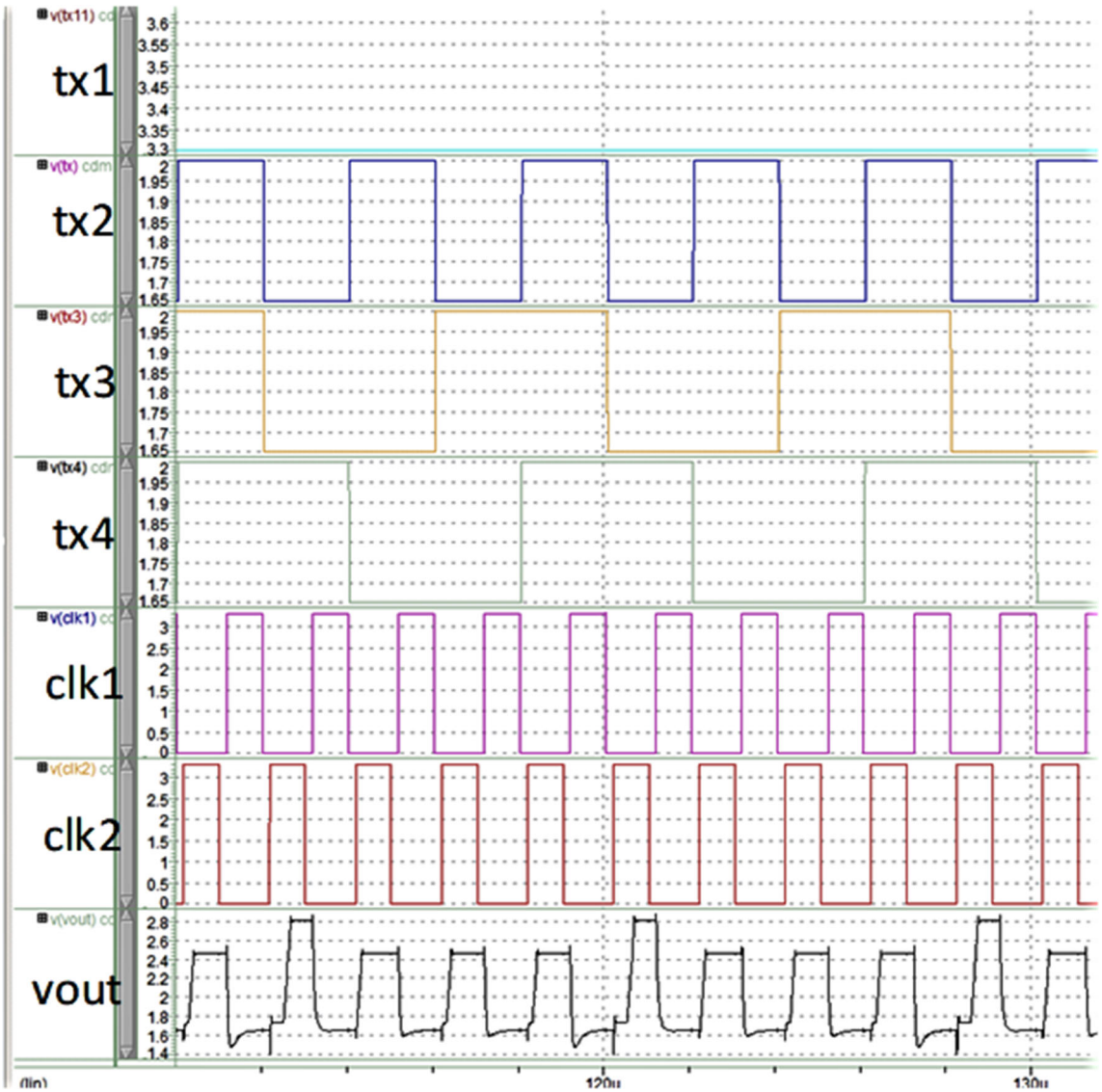

Fig. 9 Simulation results on the timing logic circuit for TX channels and the CA (charge amplifier) output

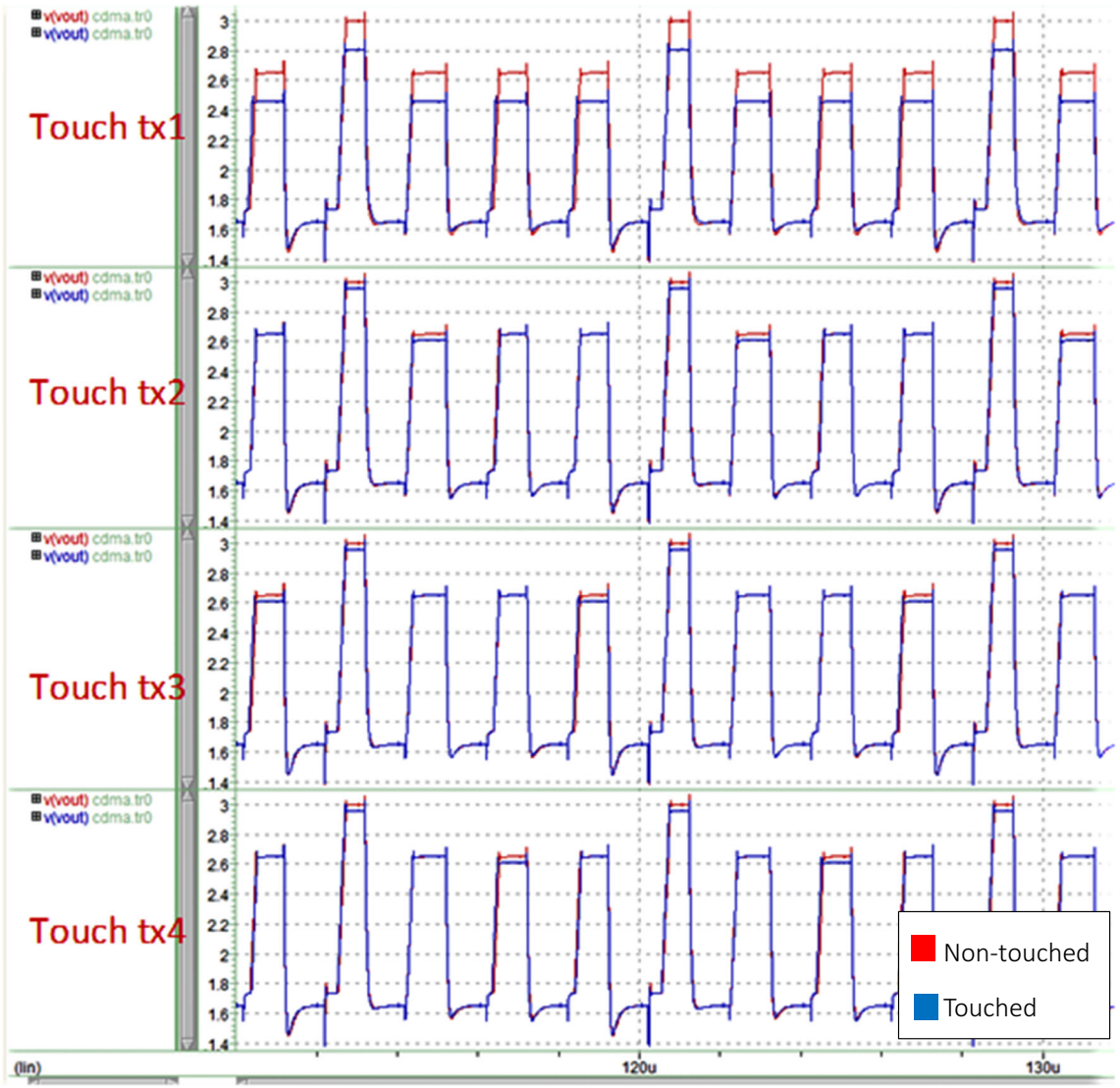

Fig. 10 Simulation results of the outputs of the designed charge amplifier (CA) for the cases of touched and non-touched

Table 4 The behavior of the cases for four different Rx waveforms

	1st	2nd	3rd	4th
Touch Tx1	Drop	Drop	Drop	Drop
Touch Tx2	Drop	Drop	Unchanged	Unchanged
Touch Tx3	Drop	Unchanged	Unchanged	Drop
Touch Tx4	Drop	Unchanged	Drop	Unchanged

3 Readout circuitry

The entire readout circuitry for the touch sensing panel is illustrated by the blocks in Fig. 6, where there are the analog part with multiple charge amplifiers driven by the approach of code-division multiple-sensing (CDMS) and then a digital unit with algorithms to detect touches.

3.1 Driving the TSP using code division multiple access

The method of code-division multiple-sensing (CDMS) is employed in this work, with an expectation to deliver better performance than the conventional time-interleaved sensing method. By Parseval's theorem, to obtain higher SNR for the touch-screen panel (TSP) system with a wideband noise distribution, the power spectral density of the signal should be higher, which inevitably needs longer access time (Shin et al. 2013). However, it can be overcome by adopting a CDMA technique, which is a well-established method in RF communication systems.

If the driving signals of the TSP is presented as a matrix, a traditional time-interleaved sensing method is a unit matrix. In this study, the traditional driving unit matrix is replaced with the Walsh–Hadamard transform matrix, which is one of well-known CDMA approaches. The Walsh transform method, as shown in Fig. 7, offers faster driving for capacitive sensing than the time-interleaved matrix does, since it sends multiple TX electrodes simultaneously and decodes all the RX signals at once to decipher the touch location, significantly shorten the time needed to complete sensing over a TSP. Table 3 summarizes the comparison in performance between CDMA and Time-interleaved sensing. It is seen from this table that although the design and implementation of CDMA is more complicated than the conventional time-interleave sensing, the properties of orthogonality by CDMA makes possible to eliminate effectively the inter-channel noise.

3.2 Analog front-end

The analog front-end of the readout circuitry designed by this study consists mainly of multiple switched-capacitor charge amplifier (CA), as shown in Fig. 8. The charge amplifier (CA) has been widely used for detecting capacitive changes due to its high accuracy and linearity. Furthermore, this circuit can attenuate touch screen environment noise like a band-pass filter. In this work, four charge-amplifiers are designed to sense the variation of the mutual capacitances as shown in Fig. 8. Each sensing channel of the TSP, RX, is connected with a charge amplifier. The charge amplifiers sense the output at RXes and then convert them to voltage signals with amplitudes that are proportional to the mutual capacitances, C_{m}'s. In Fig. 8, when clk1 turns on and clk2 turns off, the input voltage from TXes enforces the charge to be stored in C_{m}, the mutual capacitance between TX and RX electrode layers. When clk1 turns off and clk2 turns on, the charges in the mutual capacitor are discharged to C_{FB}, generating the voltage change proportional to the capacitance change, yielding

$$V_{CA} = V_{in}\frac{c_m}{c_{FB}}, \tag{4}$$

where V_{CA} id the output voltage of the charge amplifier while V_{in} is the input voltage to a given TX. In addition to CAs, a switch timing logic circuit is orchestrated used to generate time-synchronized driving signals on all switches of the switched-capacitor (SC) circuits to finally output signals to RXes. The output signals at RXes are next decoded based on the Walsh CDMA coding scheme to determine the voltage variation of all the mutual capacitances between all TXes and RXes. Simulations are conducted using HSPICE to validate the expected performance before experiment. Figure 9 show the simulated TXes, clks and the output voltage of the designed charge amplifier at RX1 with touching. It can be seen from this figure that all four TX signals do follow the Walsh code waveforms designed as shown in Fig. 7, while the output at RX shows a sequence of high, low, low and low, corresponding

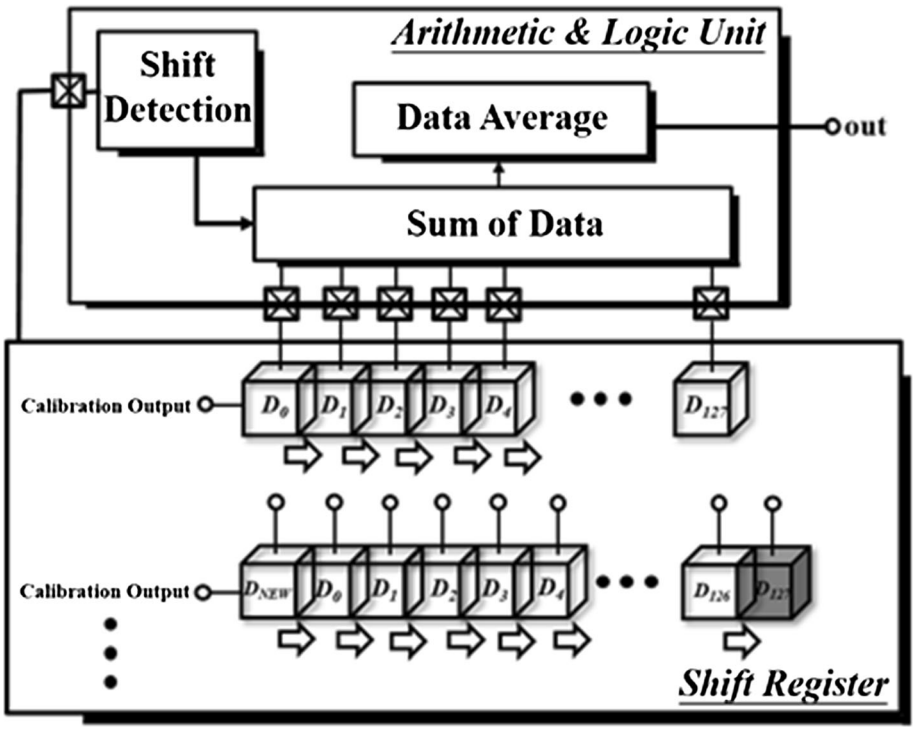

Fig. 11 The data-flow of the designed moving averaging

Table 5 Measured mutual capacitances of the on-cell touch panel

	R16/27	R15/28	R14/29	R13/30	R12/31	R11/32	R10/33	R9/34	R8/35	R7/36	R6/37	R5/38	R4/39	R3/40	R2/41	R1/42
T1/3	3.573	3.421	3.426	3.46	3.422	3.42	3.446	3.47	3.437	3.452	3.509	3.481	3.473	3.44	3.434	3.486
T2/4	3.357	3.253	3.215	3.21	3.263	3.231	3.224	3.239	3.199	3.266	3.243	3.2963	3.297	3.269	3.288	3.386
T3/5	3.335	3.23	3.219	3.18	3.242	3.252	3.23	3.215	3.249	3.271	3.252	3.301	3.267	3.326	3.327	3.444
T4/6	3.335	3.241	3.225	3.194	3.348	3.275	3.266	3.206	3.249	3.295	3.261	3.313	3.313	3.313	3.341	3.351
T5/7	3.359	3.266	3.211	3.235	3.232	3.243	3.219	3.216	3.298	3.262	3.254	3.264	3.339	3.254	3.37	3.427
T6/8	3.355	3.228	3.265	3.255	3.268	3.251	3.273	3.258	3.252	3.277	3.231	3.263	3.256	3.343	3.305	3.425
T7/9	3.33	3.281	3.216	3.221	3.297	3.227	3.291	3.254	3.272	3.283	3.257	3.252	3.306	3.308	3.295	3.339
T8/10	3.368	3.273	3.234	3.242	3.247	3.2223	3.221	3.26	3.275	3.246	3.282	3.289	3.271	3.252	3.334	3.408
T9/11	3.321	3.205	3.28	3.235	3.235	3.302	3.192	3.212	3.266	3.275	3.319	3.259	3.291	3.293	3.295	3.348
T10/12	3.318	3.22	3.213	3.269	3.188	3.219	3.267	3.3	3.241	3.253	3.29	3.236	3.239	3.285	3.318	3.326
T11/13	3.317	3.291	3.217	3.271	3.283	3.223	3.132	3.219	3.242	3.29	3.307	3.294	3.293	3.281	3.266	3.37
T12/14	3.386	3.206	3.274	3.237	3.301	3.225	3.282	3.2222	3.238	3.279	3.266	3.238	3.306	3.315	3.285	3.341
T13/15	3.392	3.253	3.193	3.207	3.238	3.244	3.283	3.259	3.214	3.264	3.21	3.3	3.27	3.302	3.256	3.429
T14/16	3.287	3.217	3.24	3.24	3.24	3.308	3.256	3.235	3.281	3.226	3.244	3.258	3.236	3.266	3.333	3.406
T15/17	3.349	3.3	3.224	3.224	3.206	3.261	3.268	3.288	3.268	3.275	3.279	3.278	3.279	3.23	3.315	3.392
T16/18	3.318	3.215	3.268	3.24	3.269	3.238	3.237	3.27	3.219	3.248	3.266	3.266	3.279	3.301	3.319	3.371
T17/19	3.352	3.252	3.241	3.211	3.282	3.28	3.241	3.233	3.23	3.309	3.243	3.298	3.291	3.289	3.289	3.373
T18/20	3.38	3.222	3.255	3.216	3.243	3.256	3.235	3.281	3.226	3.244	3.258	3.236	3.266	3.333	3.306	3.426
T19/21	3.327	3.314	3.267	3.223	3.235	3.194	3.192	3.276	3.28	3.22	3.304	3.289	3.265	3.283	3.321	3.389
T20/22	3.388	3.274	3.277	3.249	3.3	3.245	3.242	3.25	3.262	3.279	3.262	3.292	3.301	3.294	3.278	3.376
T21/23	3.373	3.226	3.246	3.28	3.308	3.222	3.28	3.287	3.236	3.216	3.272	3.284	3.277	3.226	3.309	3.391
T22/24	3.605	3.553	3.474	3.515	3.495	3.491	3.539	3.474	3.42	3.454	3.512	3.56	3.52	3.484	3.581	3.797

exactly to the driving waveform of TX1, [1, 1, 1, 1], TX2, [1, 1, − 1, − 1], TX3, [1, − 1, − 1, 1] and TX4, [1, − 1, 1, − 1], as given in Fig. 7, respectively. Simulation works are next extended to the cases of touches, considering a finger touching the cross point between TX/RX electrodes to change the mutual capacitance between TX1 and RX1 from 3 to 2.7 pF. The results are shown in Fig. 10, where the drops in the output voltage level from CA at RX1 from red waveforms to blue are seen as in the sensed waveforms with the finger touching TX1/RX1. Similarly, some other voltage drops are seen as the finger touching TX2, TX3 and TX4. It is found that the drops or unchanged follow exactly the scheme of the Walsh CDMA code, as listed in Table 4, validating the effectiveness of the designed analog front-end circuit for touch sensing. With successfully design of the analog front-end, the back-end digital algorithm is designed next to filter the noise, detect the touch position and then report the correct touch position.

3.3 Digital circuits

A digital unit, as shown in Fig. 6, with algorithms designed to determining if there is a touch is orchestrated and realized by this study. This digital circuit plays an important role in calibrating the non-uniform baseline of touch panel, owing to process variations. First, a timing switching logic

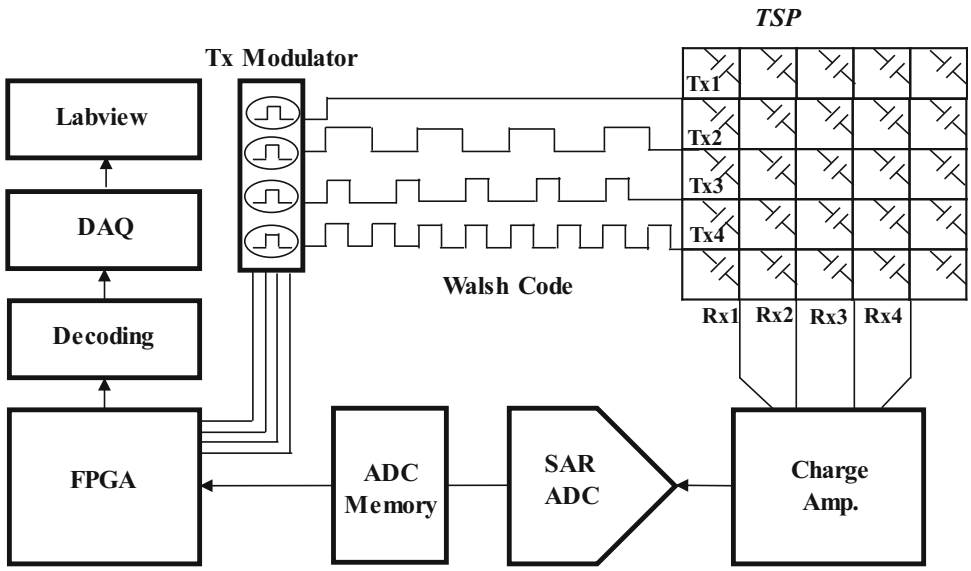

Fig. 12 The architecture of the designed touch readout circuitry

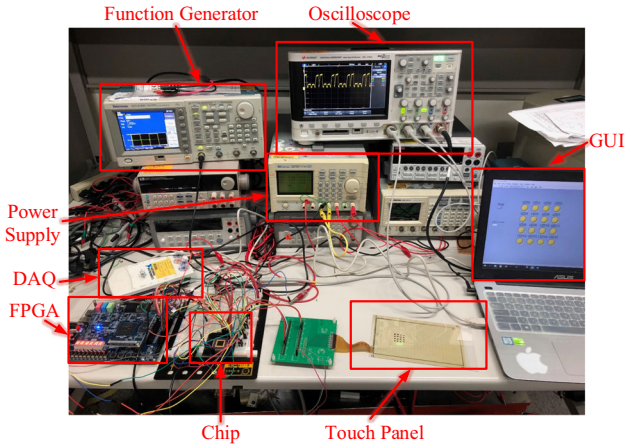

Fig. 13 The experimental setup for testing the designed touch readout circuit

is designed to generate the driving signals based on CDMA Walsh code to drive TX lines. Second, an algorithm of moving average is forged towards high SNR to enhance both effectiveness and sensitivity of touch detection. Note that the algorithm of moving average is commonly used to reduce uncorrelated noises while retaining sharp step responses (Smith 1999). The computation of moving average follows

$$y_i = \frac{1}{M}\sum_{j=-\frac{M-1}{2}}^{\frac{M-1}{2}} x_{i+j}dx, \tag{5}$$

where y_i is output signal, x_{i+j} is the input signal, and M is the number of points used in the moving average. As the number of points M in the filter increases, the noise becomes lower, while the edges become less sharp. To design the best moving averaging, the edge sharpness of the output signal is necessary to be concerned. Under fixed edge sharpness condition, the number of points utilized in the moving averaging can be determined. The data flow and related computations for the moving averaging is shown in Fig. 11. The shift register is employed to obtain 50 input data, while the arithmetic and logic units are used for calculations including the sum of data and averaging to enhance the quality of the final output signal for determining touches. Note that since the operating frequency of sensing touch signal is above 10 kHz. With M being designed as 50, the latency is about 24.5, then the frame rate of the touching sensing can be up to 10 kHz/24.5 = 408 Hz, which is well beyond 240 Hz normally required by most of current display systems. The next step is to design the CDMA algorithm. Towards this end, the output waveforms of the circuit is orchestrated first, which is obtained by analyzing the difference in the touched and non-touched waveforms and setting a threshold voltage.

4 Experimental results

4.1 Measuring capacitances of the proposed touch panel

The expected performance of the designed touch panel is validated by the measurement on the mutual capacitance between electrodes from an LCR meter. The results are shown in Table 5, indicating that the mutual capacitance of each intersection point is about 3 pF in average, which is acceptable for quality touch detections.

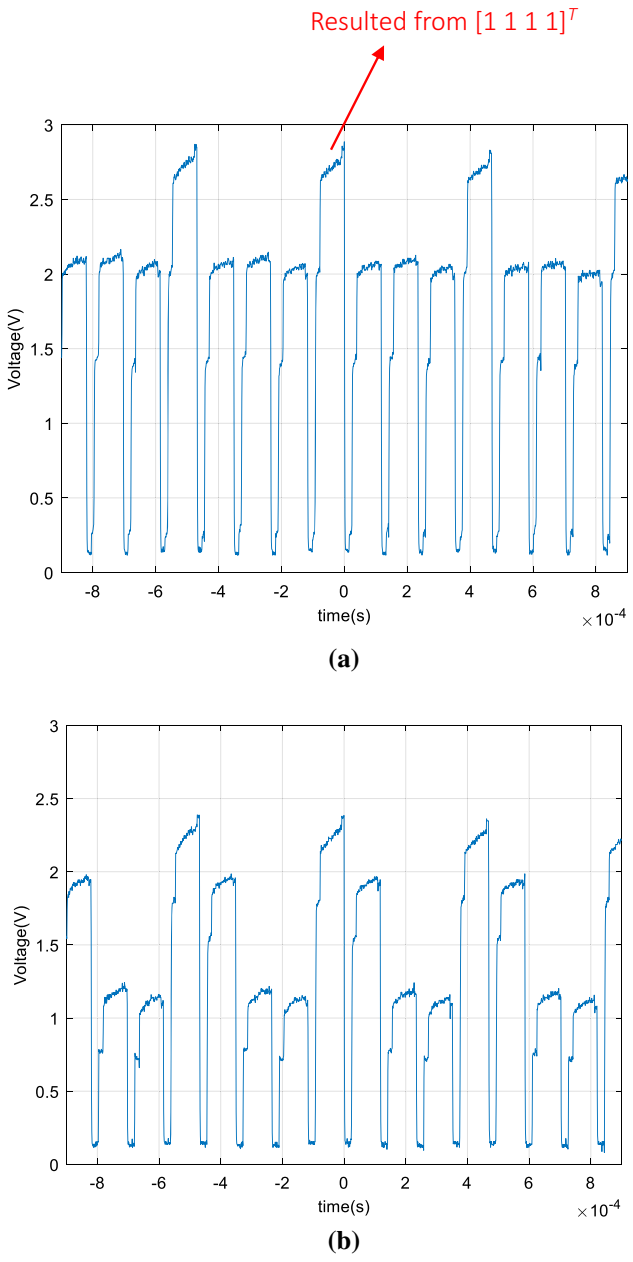

Fig. 14 Experimental output waveforms read by **a** the non-touched RX1; **b** the non-touched RX2; **c** the non-touched RX3; **d** the non-touched RX4

4.2 Experimental Results of Readout Circuits

The experiment system for validating the performance of the designed readout IC system is shown in Fig. 12, which is composed of a switched-capacitor charge amplifier (AC), an ADC, a driving CDMA code generator and a unit of data acquisition (DAQ) for analysis. The digital unit contains a timing control, a CDMA calibration algorithm and a moving averaging unit that are implemented in the Field Programmable Gate Array (FPGA) board. A 7-inch

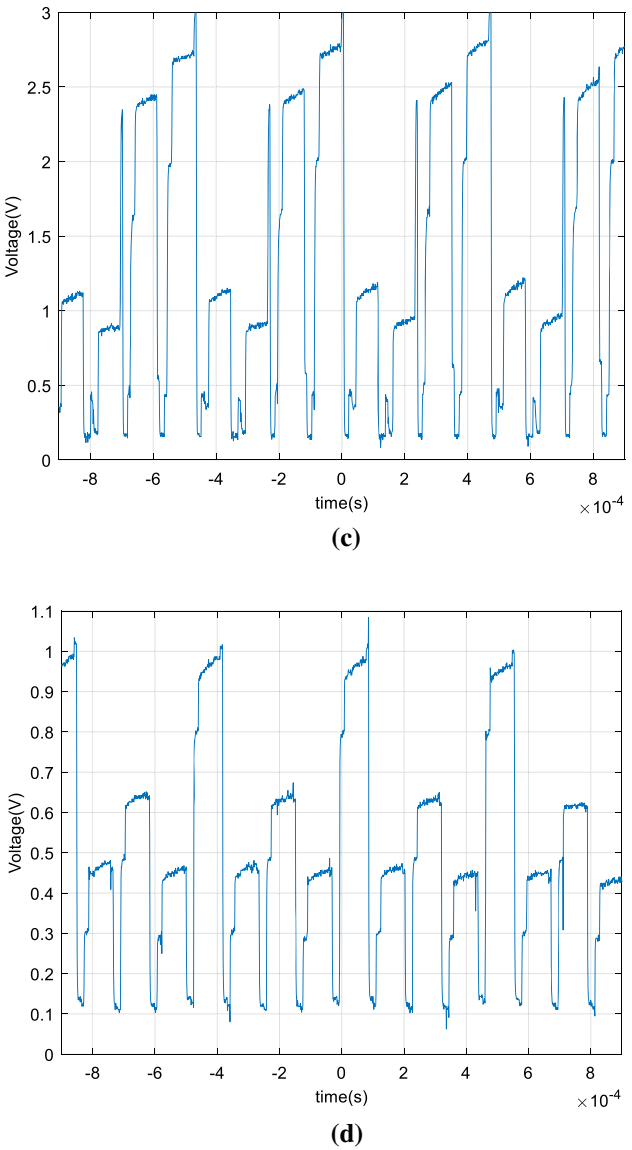

Fig. 14 continued

mutual-capacitive TSP with 22 TX channels and 16 RX channels is considered for experiments. Under the touch panel is a display to simulate realistic interfering electronic noises on the touch panel. The proposed readout circuit supports 4 driving and 4 sensing channels. Note that although the designed readout supports only partial electrodes of the considered touch panel, the test results can still provide adequate information to validate extensiveness of the achieved performance by the designed readout IC. The platform for testing the proposed readout circuit, as shown in Fig. 13, is orchestrated successfully, consisting of an FPGA board and the tape-out chip. The touched and untouched mutual capacitances of TSP are measured to be approximately 3 pF and 3.2 pF, respectively.

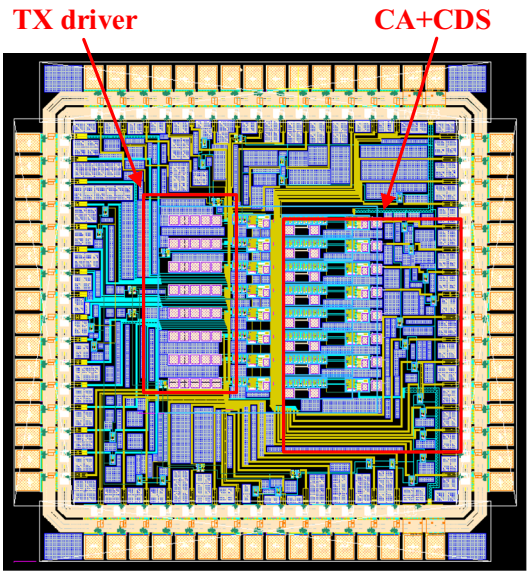

(a)

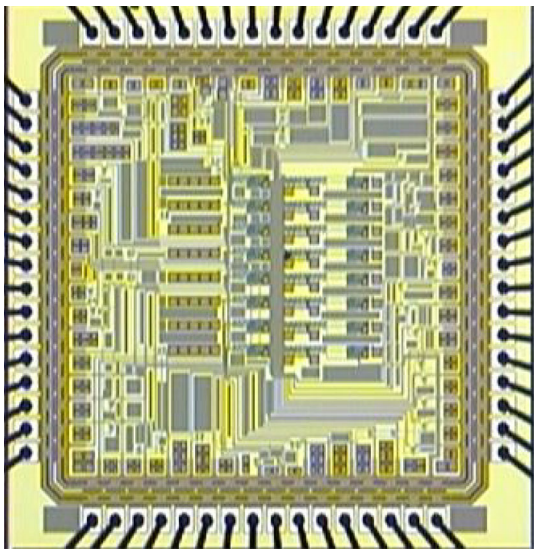

(b)

Fig. 15 **a** The layout of the designed readout chip; **b** the microphoto of the designed readout IC chip

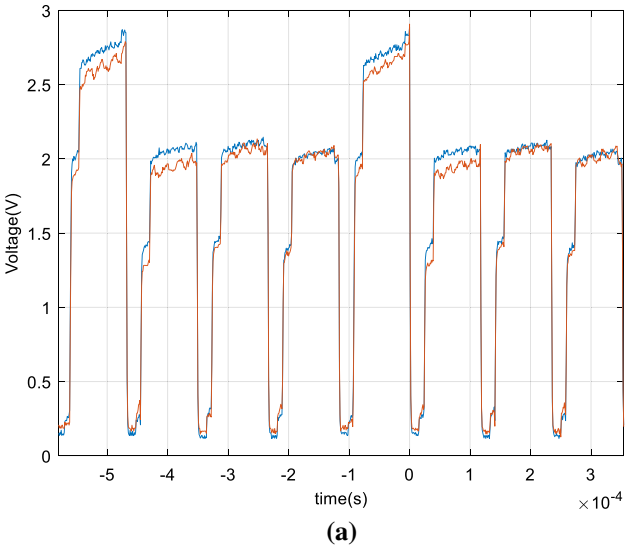

(a)

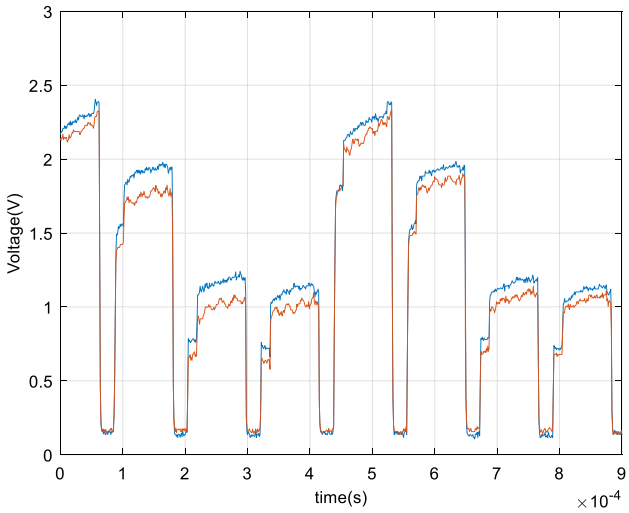

(b)

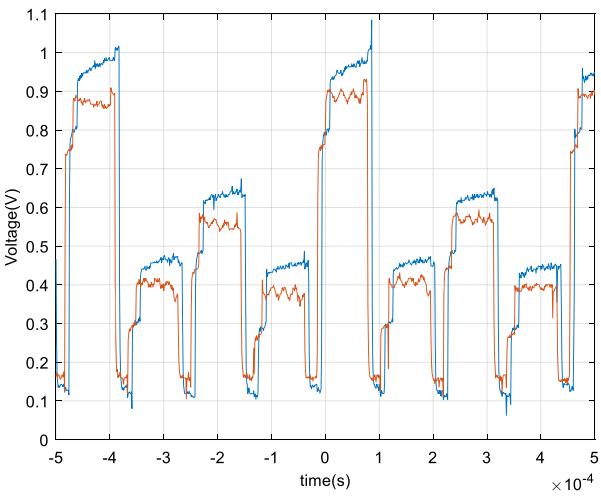

(c)

Fig. 16 The experimental waveforms received by RX electrodes ▶ using CDMA technology; **a** with a finger touching the cross point of TX2 and RX1; **b** TX1 and RX2; **c** TX1 and RX4

All the non-touched output waveform results measured from RX1 to RX4 are shown in Fig. 14a–d. The layout of the proposed IC is shown in Fig. 15a, while die micrograph is in Fig. 15b. The results in Fig. 14a shows the non-touched output waveforms of RX1 measured are the same as their simulated counterparts in Fig. 10 Based on the Walsh

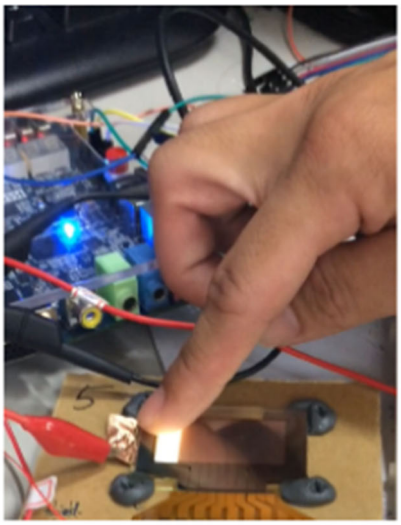

(a)

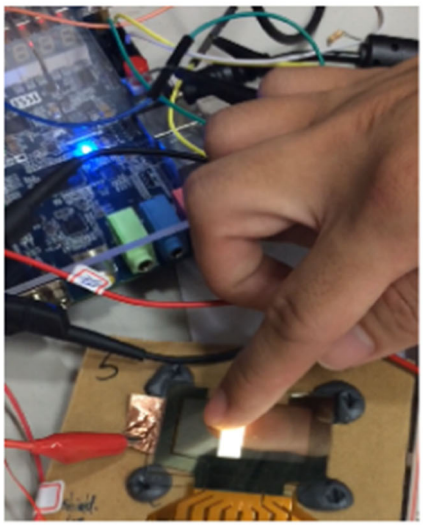

(b)

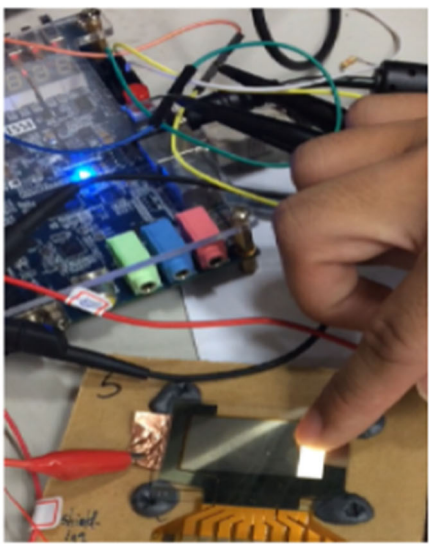

(c)

◀**Fig. 17** The testing of touches on the TSP with a display under; **a** touching the left position; **b** middle; **c** right

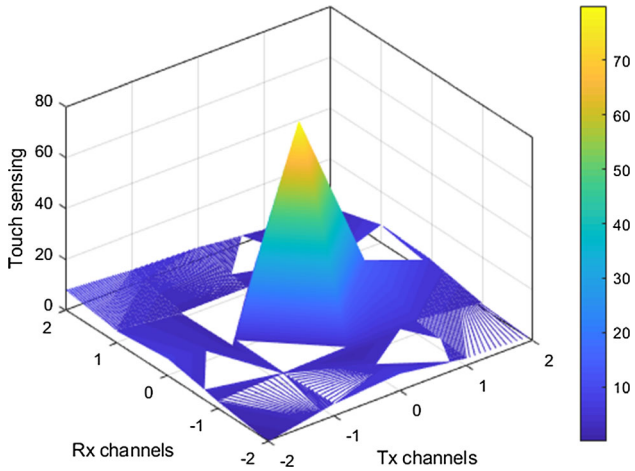

Fig. 18 The sensed touch signal at the output of the charge amplifier (CA) by the designed CDMA circuit in a 3-D view versus RX and TX channels of the TSP considered

driving waveforms in Fig. 7, RX1 responds to the driving waveforms of $[1\ 1\ 1\ 1]^T$, $[1\ 1\ -\ 1\ -\ 1]^T$, $[1\ -\ 1\ -\ 1\ 1]^T$ and $[1\ -\ 1\ 1\ -\ 1]^T$ from TX1, TX2, TX3 and TX4, respectively. Among the afore-mentioned four driving waveforms, the first $[1\ 1\ 1\ 1]^T$ should result in the highest response at the output of RX1, since there is no "− 1" in $[1\ 1\ 1\ 1]^T$ as others have, noting that "1" correspond to charging the mutual capacitance by the charge amplifier while "-1" does discharge. This is evidenced in Fig. 14a. As for the other non-touched output waveforms of RX2, RX3 and RX4, similar analysis can easily be conducted to validate the results in Fig. 14b–d.

In the next step, experiments are conducted for the cases of touches, with a display layer actually located at the bottom of touch panel screen to simulate realistic interfering electronic noises on the touch panel while a finger is touching the touch panel, as shown in Fig. 16. Figure 17 show the touched waveforms with a finger touching the cross point of TX2/RX1, TX1/RX2 and TX1/RX4. It is clearly seen from the output signal at RX1 as shown in Fig. 16a that there are substantial voltage changes at the 1st and 2nd peak, matching to the Walsh driving waveform of TX2, $[1\ 1\ -\ 1\ -\ 1]^T$, thus predicting correctly a touch TX2/RX1. Similarly, as seen in Fig. 16b, substantial voltage changes at all peaks matches the driving waveform of TX1, $[1\ 1\ 1\ 1]^T$, thus also predicting correctly a touch TX1/RX2. Also as seen in Fig. 16c, substantial voltage changes at all peaks matches the driving waveform of TX1, $[1\ 1\ 1\ 1]^T$, thus also predicting corerctly a touch at TX1/RX4.

Table 6 The performance summary of the proposed readout circuit in comparison with others

	ISSCC 10' (Kim et al. 2010)	ISSCC 13' (Yang et al. 2012)	ISSCC 13' (Shin et al. 2013)	ISSCC 16' (Jun et al. 2016)	JSSC 19' (Park et al. 2019)	This work
Process	3 V 90 nm CMOS	3.3 V 350 nm CMOS	3.3 V 180 nm CMOS	5.5 V 110 nm CMOS	3.3 V 180 nm CMOS	3.3 V 180 nm CMOS
Driving method	Interleaved	Interleaved	Simultaneous	Interleaved	Simultaneous (adiabatic)	Simultaneous
Channels	24	TX:27 RX:43	TX:30 RX:24	TX:18 RX:32	TX:16 RX:33	TX:4 RX:4
Capacitance type	Self	Mutual	Mutual	Self	Mutual	Mutual
Reporting rate	120 Hz	120 Hz	240 Hz	120 Hz	120 Hz	240 Hz
SNR	36 dB	39 dB	35 dB	48 dB	57 dB	42 dB
Power consumption@ per sensing channel	0.5 mW	0.27 mW	0.37 mW	0.4 mW	0.53 mW	0.39 mW
Chip area@ per sensing channel	0.15 mm^2	0.15 mm^2	0.275 mm^2	0.16 mm^2	0.21 mm^2	0.17 mm^2

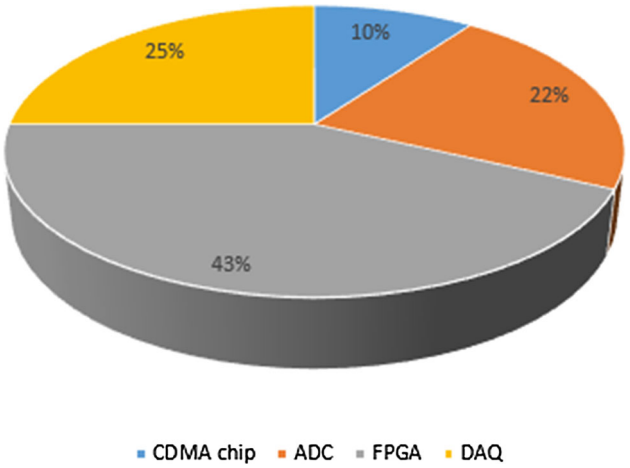

Fig. 19 Breakdown of the power consumption by the CDMA touch readout in a chart showing that 43% of the power is consumed by the FPGA which is the highest in percentage, 25% by DAQ, 22% by ADC and 10% by CDMA chip

Finally, the out signals at RX electrodes are sent to the back-end digital algorithm circuit for reducing noise, detecting and determining the touch position. A 3D touch plot for a typical touch is shown in Fig. 18 to display the changes in output voltages over the touch panel for a touch at a given location. It can be seen from this figure that a large readout signal surge is clearly seen at the touch point, reaching as high as 42 dB. Note that with the operating frequency of readout IC above 10 kHz, due to the simultaneous driving/sensing by the proposed CDMA, the sensing frequency is tuned up herein to 240 Hz. The achieved performance of the readout proposed by this study is compared to other related prior arts. The comparison is summarized in Table 6, where one can see that the proposed chip employing CDMA technology, the SNR is 42 dB, while the reporting rate is as high as 240 Hz, rendering the highest sensing speed as compared to all the other existing studies. Finally, Fig. 19 provides a power breakdown of the total power consumption in a pie chart, where the power by the CDMA is the most consuming. The investigation shows that 43% of the power is consumed by the field programmable gate array (FPGA) unit which is the highest in percentage. The unit of Data Acquisition (DAQ) consumes 25% power followed by the Analoge to Digital Converter (ADC) with 22% power consumption and 10% power consumption by CDMA chip which is the least power consumption among all.

5 Conclusion

A new readout circuit employing the method of code division multiple access (CDMA) to drive the touch panel is successfully designed and applied to a novel 7-inch ultra-thin, flexible on-cell touch panel. The work starts with the simulation via COMSOL to determine the optimal thickness of the touch panel and the size of the touch electrodes in a specially-designed pattern. Then it is followed by proposing the CDMA method to effectively eliminate the touch interference and channel interference between the electrodes. It also successfully reduces the electromagnetic interference between channels, resulting in enhancement of the touch signal. The design of switched-capacitor (SC) circuitry is applied to avoid interfering sample signals from parasitic capacitances for increasing the voltage difference resulted from capacitance changes of the touch panel due to touching. This designed readout integrated circuit (IC) is successfully fabricated using the 0.18-μm CMOS

technology offered by Taiwan Semiconductor Manufacturing Company (TSMC). The analog signals are successfully read by the ADC on an FPGA board, and then processed with moving averaging to determine if there are touches. In results, the proposed chip employing CDMA technology renders the SNR of 42 dB, the reporting rate as high as 240 Hz, the highest sensing speed as compared to all the other existing studies.

Acknowledgements The authors appreciate the supports from Industrial Technology Research Institute of Taiwan. This study is supported by Ministry of Science and Technology, Taiwan grant nos. MOST 106-2221-E-009 -089, MOST 107-2221-E-009-166 -MY2, MOST 108-2823-8-009 -002 -, MOST 108-2623-E-009 -004 –D and MOST 109-2622-8-009-018 -TE1. This work was financially supported by the "Center for Intelligent Drug Systems and Smart Biodevices (IDS^{2}B)" from The Featured Areas Research Center Program within the framework of the Higher Education Sprout Project by the Ministry of Education (MOE) in Taiwan. It was also supported in part by Hsinchu Science Park Bureau, MOST grant No. 108A31B.

References

Baier PW (1996) A critical review of CDMA. In: Proceedings IEEE 46th vehicular technology conference (VTC′96). Atlanta, pp 6–10

Barrett G, Omote R (2010) Projected-capacitive touch technology. Inf Display Mag 26–3:16–21

Chawla P, Singh B (2014) Role of walsh codes and pseudorandom noise sequence in CDMA. In: 2014 IEEE International Conference on industrial engineering and engineering management, 2014

Cordeiro C-A, Rebeschi T-J, 3 M Innovative Properties Company (2013) High speed noise tolerant multi-touch touch device and controller therefore. U.S. Patent 8411066 B2, 2013

Dieulesaint E, Royer D, Legras O, Chaabi A (1991) Acoustic plate mode touch screen. Electron Lett 27:49–51

Downs R (2005) Using resistive touch screens for human/machine interface. Technical report, Texas Instruments Incorporated, Texas Instruments, 2005

Jang Y-S, Ko Y-H, Choi J-M, Oh H-S, Lee S-G (2013) A 45-dB, 150-Hz and 18-mW touch controller for on-cell capacitive TSP systems. IEEE Trans Circ Syst 61:748–752

Jun J-H, Kim B-J, Shin S-K, Jang K, Baek J-S, Kim C (2016) In-cell self-capacitive-type mobile touch system and embedded readout circuit in display driver IC. J Display Techcol 12:1613–1622

Kim H-R, Choi Y-K, Byun S-H, Kim S-W, Choi KH, Park J-K, Lee D-Y, Wu Z-Y, Kwon H-D, Choi Y-Y, Lee C-J, Cho H-H, Yu J-S, Lee M (2010) A mobile-display-driver IC embedding a capacitive-touch screen controller system. In: IEEE ISSCC, 2010

Ko SH (2020) "A-24 dB in-band noise-immunity mutual capacitance readout system for variable refresh rate of active-matrix OLED display. In: IEEE Transactions on circuits and systems I: regular papers, 2020

Ko S-H, Shin H, Lee J, Jang H, So B-C, Yun I, Lee K (2010) Low noise capacitive sensor for multi-touch mobile handset's applications. In: IEEE ASSCC, pp 1–4, 2010

Martin S-J, Verschoor G-L-B, Webster M-A, Walker A-B (2002) The internal electric field distribution in bilayer organic light emitting diodes. Org Electron 3:129–141

Park J, Hwang YH, Oh J, Song Y, Park JE, Jeong DK (2019) A mutual capacitance touch readout IC with 64% reduced-power adiabatic driving over heavily coupled touch screen. IEEE J Solid-State Circ 54(6):1694–1704

Shin H, Ko S, Jang H, Yun I (2013) A 55 dB SNR wih 240 Hz frame scan rate mutual capacitory 30x24 touch-screen panel read-out IC using code-division multiple sensing technique. In: IEEE ISSCC, 2013

Smith S-W (1999) The Scientist's and engineer's guide to digital signal processing, 2nd edn. California Technical Publishing, San Diego, California, pp 277–284

Xing H, Deng L, Ke J, Yu T, Liao C, Luo H, Huang S (2019) High sensitive readout circuit for capacitance touch panel with large size. IEEE Sens J 19(4):1412–1415

Yang J-H, Park S-H, Jeon JY, Kim HS, Park CB, Lee JC, Kim JW, Cho GH (2012)A high-SNR area-efficient readout circuit using a delta- integration method for capacitive touch screen panels. In: Soc. Inf. Display (SID) Symp. Digest, pp 1570–1573, June 2012